

Scaling of Disorder Operator and Entanglement Entropy at Easy-Plane Deconfined Quantum Criticalities

Jiarui Zhao,^{1,*} Zi Yang Meng,^{1,†} Yan-Cheng Wang,^{2,3,‡} and Nvsen Ma^{4,§}

¹*Department of Physics and HKU-UCAS Joint Institute of Theoretical and Computational Physics, The University of Hong Kong, Pokfulam Road, Hong Kong SAR, China*

²*Hangzhou International Innovation Institute, Beihang University, Hangzhou 311115, China*

³*Tianmushan Laboratory, Hangzhou 311115, China*

⁴*School of Physics, Beihang University, Beijing 100191, China*

(Dated: June 6, 2024)

We systematically investigate the scaling behavior of the disorder operator and the entanglement entropy (EE) of the easy-plane JQ (EPJQ) model at its transition between the antiferromagnetic XY ordered phase (AFX) and the valence bond solid (VBS) phase. We find **(1)** there exists a finite value of the order parameters at the AFX-VBS phase transition points of the EPJQ model, and the finite order parameter is strengthened as anisotropy Δ varies from the Heisenberg limit ($\Delta = 1$) to the easy-plane limit ($\Delta = 0$); **(2)** Both EE and disorder operator with smooth boundary cut exhibit anomalous scaling behavior at the transition points, resembling the scaling inside the Goldstone model phase, and the anomalous scaling becomes strengthened as the transition becomes more first order; **(3)** First put forward in Ref. [arXiv:2401.12838], with the finite-size corrections in EE for Goldstone phase is properly considered in the fitting form, the anomalous scaling behavior of EE can be adapted with emergent SO(5) symmetry breaking at the Heisenberg limit ($\Delta = 1$). We extend this method in the EPJQ model and observe similar results, which may indicate emergent SO(4) symmetry breaking in the easy-plane regime ($\Delta < 1$) or emergent SO(5) symmetry breaking in the Heisenberg limit ($\Delta = 1$). These observations provide evidence that the Néel-VBS transition in the JQ model setting evolves from weak to prominent first-order transition as the system becomes anisotropic, and the non-local probes such as EE and disorder operator, serve as the sensitive tool to detect such salient yet fundamental features.

I. INTRODUCTION

The conventional Landau-Ginzburg-Wilson (LGW) paradigm for characterizing phases and their transitions has been confronted with the notion of deconfined quantum critical points (DQCPs), which describes a direct continuous transition between Néel ordered phases and valence-bond-solid (VBS) phases [1–4]. However, the feasibility of realizing such transitions in lattice models remains a contentious issue because of the observation of anomalous behavior against conformal field theories (CFT) [5–17], such as drifting of critical exponents [5–7], possible violation of CFT bounds [8–10], and the anomalous scaling behavior of entanglement entropies and disorder operators [11–17]. A deeper exploration of the origins of these anomalous behaviors will benefit not only the better understanding of nature of DQCPs but also its lattice model and even material realizations [18–23].

Among all the anomalous behavior against CFTs, we are in particular interested in the anomalous finite-size scaling behavior of Rényi EE and disorder operator, as it happens even at relatively small system sizes [11–17] where other physical quantities such as order parameters and correlation functions still exhibit good agree-

ment with a continuous phase transition [24–28]. In fact, at the DQCPs of SU(2) JQ₂ and JQ₃ models, our previous works [11–14] show that disorder operator and EE all exhibit anomalous scaling against CFTs. To be specific, for the corner cut case where the boundary of subregion has four $\frac{\pi}{2}$ corners, both disorder operator and EE have a positive logarithmic correction to the leading order area law term which violates the unitary CFT prediction that the correction must be negative [29–31]. Later, further studies clarified that the violation of EE actually arises from the smooth part of the subregion. In fact, for smooth cut case where the boundary has no sharp corners, the anomalous logarithmic subleading correction also exists in EE, which is incompatible with CFTs [13, 14], but seems to be more compatible with the existence of Goldstone modes [32, 33] and can also possibly be adapted with the ‘walking’ pseudo-criticality behavior at the transition [34–37]. In addition, recently another work [38] shows that scaling of EE at the DQCP is cut-dependent, and the anomalous log correction for smooth cut can be suppressed by considering a tilted square lattice by $\frac{\pi}{4}$ degrees, and the essential information of the CFTs might be captured by this cut at small system sizes. In this context, the scalings of these nonlocal physical observables prove to be powerful and sensitive tools for diagnosing the various possible scenarios of the DQCPs [11–14, 33] and revealing the universal information of the possible CFT nearby the transitions [38].

Here in this work, we aim to shed more insights on this issue by tuning the JQ-type Néel-VBS transition

* jrzhao@connect.hku.hk

† zymeng@hku.hk

‡ ycwangphys@buaa.edu.cn

§ nvsenma@buaa.edu.cn

from weakly first-order to a more prominent first-order transition, such that many of the salient features observed at the SU(2) JQ limit, for example, the anomalous finite-size scaling behavior in the entanglement entropy (EE) [12–14, 33] and disorder operator [11], can also be examined at a clear first-order transition, and the connection between the observed anomalous behavior in EE and disorder operator with the first-order nature of the transitions can be further clarified. A possible platform to achieve this goal is the easy-plane JQ (EPJQ) model, which adds the easy-plane anisotropy to the Heisenberg term in the JQ model, as shown in Eq. (1), to tune the Néel-VBS transition to be more first-ordered. Previous studies have investigated the nature of the Néel-VBS transition at different anisotropy Δ , both in 2D and 3D lattice model settings [21, 28, 39–41], and the general expectation/observation is that the more Δ tunes away from the Heisenberg limit ($\Delta = 1$) towards the easy-plane limit ($\Delta = 0$), the stronger the first order of the Néel-VBS transition. The EPJQ model thus serves as an ideal platform to study the anomalous scaling behavior of EE and disorder operator at these transition points simply by tuning the values of Δ .

In this paper, we use the stochastic series expansion (SSE) quantum Monte Carlo (QMC) methods [42, 43] to systematically study the order parameter, entanglement entropy, and disorder operator at the transitions of the EPJQ model. We carefully analyze the remaining ordered moments at the transitions and systematically study the evolution of the scaling of entanglement entropy and disorder operator along the transition line, as a function of Δ in Eq. (1). Our major findings are

1. For $\Delta \in [0, 1)$ there always exist finite value of the order parameters at the Néel-VBS phase transitions of the model (including the finite order parameter at the $\Delta = 1$ limit [44]), indicating the first-order nature of the transition, and the moment increases as Δ is tuned from 1 to 0;
2. Both EE and disorder operator with smooth boundary cut exhibit anomalous scaling behavior at the transition points, resembling the scaling inside the Goldstone model phase, and the anomalous scaling becomes strengthened as the transition becomes more first order;
3. Pioneered in Ref. [33, 45], with the finite-size corrections in EE for Goldstone phase is properly dealt with, the anomalous scaling behavior of EE can be adapted with emergent SO(5) symmetry breaking at the Heisenberg limit ($\Delta = 1$). We extend this method in EPJQ model and observe similar but weaker results which may indicate emergent SO(4) symmetry breaking in the easy-plane regime ($\Delta < 1$) or emergent SO(5) symmetry breaking in the Heisenberg limit ($\Delta = 1$).

Our work thus provides a comprehensive study of the scaling of EE and disorder operator along varying Δ from

1 to 0 where the weakly first-order transition is gradually tuned to a prominent first-order one. We show that the anomalous scaling of EE and disorder operator is related with the first order behavior, proving a strong evidence that the DQCP of JQ model is indeed a weakly-first-order transition and the anomalous log-corrections are from Goldstone modes. Apart from this, our work supports the idea in Ref. [33] that the origin of anomalous scaling of EE at the transition of $\Delta = 1$ is from the a continuous SO(5) symmetry breaking and the Goldstone modes associated with it. However, we do not observe the same good convergence behavior to exact number of Goldstone modes required by the SO(5) symmetry breaking at $\Delta = 1$ or SO(4) symmetry breaking at $\Delta < 1$, which might originate from insufficient data quality and the less pronounced emergent SO(4) symmetry in the easy-plane case. Despite that, our results strongly suggest that the DQCPs of EPJQ model is first-order and scaling of EE and disorder operator serve as sensitive tool for detecting such transitions.

The rest of the paper is organized as follows. In Sec. II, we first introduce the EPJQ model and discuss how we extract the finite order parameters at its transition points, then we move on to the discussion of disorder operator in Sec. III and reveal its anomalous scaling in comparison with that of the conventional (2+1)D O(3) QCP and Néel phase, next we discuss the results of EE at the EPJQ transitions in Sec. IV and point out its anomalous scaling which might stem from the Goldstone mode at the first-order transition points, finally we give a comprehensive summary on our results, discuss the relation of our work with other recent works [33, 38] and point out future directions in Sec. V. Detailed analysis of the determination of the transition points and extrapolations of the order parameter, and the analysis of the quality of the fitting in EE data are presented in the Supplemental Material (SM) [46].

II. MODEL AND PHASE DIAGRAM

We study the easy-plane JQ₃ (EPJQ) model [21, 28, 39–41] as illustrated in the left inset of Fig. 1 (a) with the following Hamiltonian

$$H = J \sum_{\langle ij \rangle} (S_i^x S_j^x + S_i^y S_j^y + \Delta S_i^z S_j^z) - Q \sum_{\langle ijklmn \rangle} P_{ij} P_{kl} P_{mn}, \quad (1)$$

where $P_{ij} = \frac{1}{4} - \mathbf{S}_i \cdot \mathbf{S}_j$ is the two-spin singlet projector. For $\Delta = 1$, the model goes back to JQ₃ with isotropic Heisenberg interactions. It was found the quantum phase transition in the JQ₃ model between the Néel and VBS phases at $q_c = 0.59864(5)$ (with $q = \frac{Q}{J+Q}$ and $J+Q = 1$ as the energy unit) [11, 25], but more numerical evidence, especially from the entanglement witnesses such as EE [12–14] and disorder operator [11], reveal an anomalous subleading log-correction even if the partitioning of the lattice is smooth, i.e. no sharp corners on the

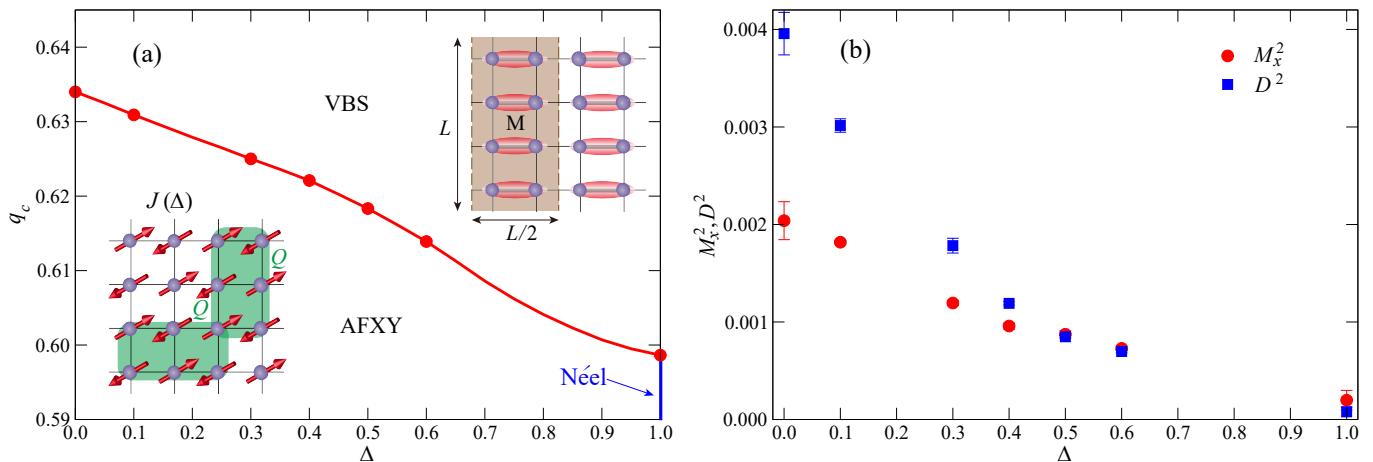


FIG. 1. (a) Ground state phase diagram of the easy-plane JQ_3 model. The red dots are critical points q_c determined from FSS analysis of Binder cumulants for different Δ values. When $\Delta = 1$, the model is the standard JQ_3 model and the weakly-first-order transition point [44] separates the Néel order state with the VBS state. At finite Δ , the antiferromagnetic Néel order is of the XY type. The Néel-VBS transition becomes prominently first order as Δ goes from 1 to 0. The insets exhibit the EPJQ model (left) and the entanglement region with smooth boundaries (right). (b) The non-zero order parameters for both AFXY and VBS phases at $q_c(\infty)$ with Δ changes from 0 to 0.6. At $\Delta = 1$, the extrapolated order parameters are from Ref. [44] of JQ_2 model.

boundary. If the transition is indeed continuous and acquires a unitary conformal field theory (CFT) description, one shall not see the log-correction with smooth boundary [13]. The fact that the sign of the observed log-coefficient is consistent with that of the presence of the Goldstone mode, further suggests there exist finite antiferromagnetic moment, i.e. remaining of the Néel order, at the transition point [32]. Such evidence promotes the understanding that the Néel-VBS transition is first order, despite being very weak at the $SU(2)$ limit [44]. In this work, we will monitor the behavior of the transition as the anisotropy in Eq. (1) is tuned away from the Heisenberg limit.

At each $\Delta \in [0, 1)$, the phase transition at zero temperature happens between the antiferromagnetic XY (AFXY) and VBS phase when tuning $q = Q/(J + Q)$ from zero to q_c . We focus on the criticality and perform SSE-QMC simulations on the EPJQ model at $\beta = 2L$ for different system sizes $L = 16, 24, 32, 48, 64, 96, 128$ with $\Delta = 0, 0.1, 0.3, 0.5$ and 0.6 . In the AFXY phase, the order parameter should be the sublattice magnetization which breaks the $U(1)$ symmetry, whose x component is defined as

$$M_x = \frac{1}{N} \sum_{i=1}^N (-1)^{x_i+y_i} S_i^x \quad (2)$$

with $\{x_i, y_i\}$ the coordinates of site i in the lattice. In the simulation with finite system sizes the expectation value of $\langle M_x^2 \rangle$ can be viewed as the square of the AFXY order parameter, whereas $\langle M_x \rangle = 0$ for finite size.

For the VBS phase, the valence bond can form in horizontal and vertical directions as exemplified of the former in the right inset of Fig. 1 (a), which can be described

through observable

$$\begin{aligned} D_x &= \frac{1}{N} \sum_i (-1)^{x_i} S_{x_i, y_i} \cdot S_{x_i+1, y_i}, \\ D_y &= \frac{1}{N} \sum_i (-1)^{y_i} S_{x_i, y_i} \cdot S_{x_i, y_i+1}, \end{aligned} \quad (3)$$

with $\{x_i, y_i\}$ the coordinates of site i . In this way, the expectation value of the square of the order parameter in VBS phase is $\langle D^2 \rangle = \langle D_x^2 \rangle + \langle D_y^2 \rangle$.

We thus perform the finite-size scaling (FSS) analysis of $\langle M_x^2 \rangle$ and $\langle D^2 \rangle$ to determine the transition points at the thermodynamic limit (TDL) [47]. The dimensionless quantity Binder cumulants are widely used in the FSS. For those two ground states in our study, the Binder cumulants are defined as

$$\begin{aligned} U_M &= 2 \left(1 - \frac{\langle M_x^4 \rangle}{3 \langle M_x^2 \rangle^2} \right), \\ U_P &= 2 \left(1 - \frac{\langle D^4 \rangle}{2 \langle D^2 \rangle^2} \right), \end{aligned} \quad (4)$$

where normalization factors and constants in Eq. (4) are decided from the degree of freedom and number of components for order parameters. Under this definition, $U_M \rightarrow 1$ in AFXY while it is zero in the VBS state when $L \rightarrow \infty$. On the contrary, in AFXY phase $U_P \rightarrow 0$ and $U_P \rightarrow 1$ in the VBS phase. Besides, both U_M and U_P are dimensionless quantities whose value are independent of system sizes at critical points. In this way, for different simulated systems $U_M(q, L_1) = U_M(q, L_2)$ and $U_D(q, L_1) = U_D(q, L_2)$ at critical point q_c , which means that the q dependence of Binder cumulants for different sizes should cross with each other at the critical point.

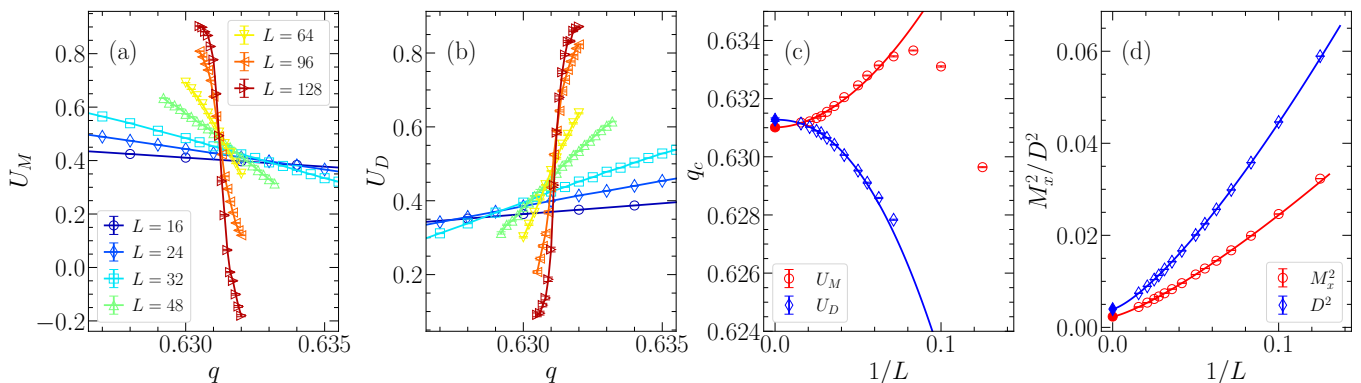


FIG. 2. The size dependence of crossing points of Binder cumulant of (a) Néel and (b) VBS order parameter in easy-plane JQ₃ model for $\Delta = 0.1$. The fact $U_M(L = 128)$ becomes negative close to the transition suggests its first-order nature. (c) The critical points at the thermodynamic limit for $1/L = 0$ are obtained through the crossing point analysis of all the $q_c(L)$ using Eq. (5). (d) The Néel and VBS order parameters as functions of $1/L$ at $\Delta = 0.1$ with the residual order at the thermodynamic limit. All the residual moments of EPJQ model in Fig. 1 (b) are obtained in this way.

	$\Delta = 0$	0.1	0.3	0.4	0.5	0.6
q_c using U_M	0.6340(1)	0.63091(5)	0.6250(2)	0.6221(2)	0.61833(6)	0.6139(3)
q_c using U_D	0.6341(5)	0.6311(9)	0.6261(4)	0.6225(2)	0.61883(5)	0.6142(1)

TABLE I. The critical points obtained from the Binder cumulants of U_M and U_D as shown in Fig. 2 for different $\Delta = 0, 0.1, 0.3, 0.4, 0.5$ and 0.6 using similar analysis in Fig. 2. The $q_c(\infty)$ of U_M and U_D are identical within two sigma. The detailed analyses are shown in Sec. I of SM [46].

Even though there only exist one phase transition point at thermodynamic limit (TDL) $q_c(\infty)$, usually all those curves will not exactly cross at $q_c(\infty)$ because of the finite size effect and corrections. Therefore, we shall locate all the crossings $q_c(L)$ where $U_M(q, L) = U_M(q, 2L)$ or $U_D(q, L) = U_D(q, 2L)$ and trace the $q_c(\infty)$ using the following scaling form

$$q_c(L) = q_c(\infty) + aL^{-1/\nu-\omega} \quad (5)$$

with ν the correlation length exponent and ω the finite-size correction exponent [28, 47, 48].

We perform such FSS analysis on the computed results in EPJQ model with different Δ . For example, the Binder cumulants of both AFXY and VBS phases close to the crossing points are presented in Fig. 2 (a) and (b) for $\Delta = 0.1$. The obtained crossings of two different curves with $(L, 2L)$ with L increasing from 8 to 64 are then illustrated in Fig. 2 (c) as well as the fitting results. Using the fitting form in Eq. (5) two $q_c(\infty)$ can be obtained with $q_c(L)$ related to different order parameters. In Fig. 2 (d), we also present the extrapolation of the ordered moments (square) of $\langle M_x^2 \rangle$ and $\langle D^2 \rangle$ at each $q_c(L)$ and eventually at the TDL, we find both $\langle M_x^2 \rangle$ and $\langle D^2 \rangle$ are finite (despite small in the y -scale of the figure) at the transition point and this is the defining evidence that the transition is first-order.

Repeating such a procedure, we can also get $q_c(\infty)$ for different Δ in Tab. I. For a given $\Delta < 1$, the $q_c(\infty)$ obtained from crossings of different dimensionless quantities agree with each other considering the error as large

as two sigma, which can be true for the continuous phase transition as well as the first-order one. However, we should point out that U_M of the AFXY order parameter for $\Delta = 0.1$ becomes negative close to q_c at the largest simulated size $L = 128$, as shown in Fig. 2 (a), the negative U_M can also be regarded as a signature of the first-order phase transition [49].

We have performed the extrapolation of the ordered moments as in Fig. 2 (d) for all the Δ values, and the obtained results are summarized in Fig. 1 (b). From which, one clearly sees that $\langle M_x^2 \rangle$ and $\langle D^2 \rangle$ are small at $\Delta = 0.6$ (they are even smaller at the isotropic limit), but they gradually increases as $\Delta \rightarrow 0$. We show all these extrapolations in the Sec. I of SM [46]. The enhancement of the ordered moments as $\Delta \rightarrow 0$ is the reason we believe along the phase AFXY-VBS phase boundary in Fig. 1 (a), the transition evolves from weakly first-order to stronger ones. As will be shown below, our non-local EE and disorder operator measurements (with smaller systems sizes than those of order parameters) successfully capture such understanding from the more traditional local measurements.

For comparison, we have also computed the disorder operator for the square lattice J_1 - J_2 Heisenberg model with the Hamiltonian

$$H_{J_1-J_2} = J_1 \sum_{\langle ij \rangle} \mathbf{S}_i \cdot \mathbf{S}_j + J_2 \sum_{\langle ij \rangle'} \mathbf{S}_i \cdot \mathbf{S}_j, \quad (6)$$

where $\langle ij \rangle$ denotes the J_1 bond and $\langle ij \rangle'$ denotes the J_2 bond. This model has a well-established (2+1)d O(3)

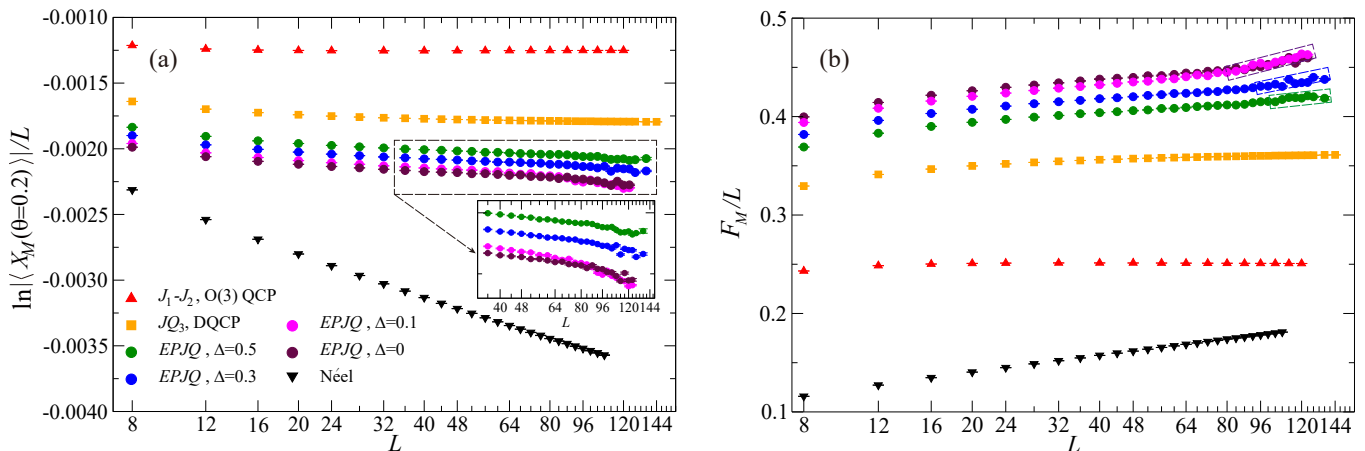


FIG. 3. (a) Disorder operator at $\theta = 0.2$ and (b) the bipartite spin fluctuations F_M as functions of system size L for the Néel phase, (2+1)D O(3) QCP of $J_1 - J_2$ model (Eq. (6)), DQCP of JQ₃ and the first-order quantum phase transition points of EPJQ (Eq. (1)), respectively. The inset in (a) and the dashed rectangular boxes in (b) show the slopes of $\ln |X_M(\theta)|/L$ and F_M became sharper as system size increases at the quantum phase transition points of EPJQ, signifying the first-order nature of the transition and such sharper slopes resemble that of the Néel phase with spontaneous symmetry breaking. (a) and (b) share the same data labeling for different models.

QCP at $(J_2/J_1)_c = 1.90951(1)$ [47] separating the Néel phase and a symmetric singlet product phase. As will also be shown below, the entanglement measurements (both disorder operator and EE) of this O(3) QCP do not have anomalous log-corrections.

III. DISORDER OPERATOR

Once the transition points of each Δ are determined, we now carry out the analysis of the disorder operator upon them. As a non-local observable, disorder operator is defined as the expectation value of a symmetry transformation applied to a finite region in the statistical or quantum many-body systems of interest [50–54]. The design and implementation of the disorder operator and the analysis of its finite size scaling behavior have been successfully carried out in the situations of spontaneous symmetry breaking phase, quantum critical points, the symmetric phases with topological orders, symmetric mass generation transition and even the free fermion surface and interacting quantum critical Fermi surface systems [11, 15, 17, 55–62].

In a 2D lattice spin model, for a region M as shown in the right inset of Fig. 1 (a), we define the U(1) disorder operator $X_M(\theta) = \prod_{i \in M} e^{i\theta(S_i^z + \frac{1}{2})}$, where S_i^z is the U(1) charge on site i . Especially for the corner region, the scaling of the U(1) disorder operator have been studied systematically [56–58, 60]. In the ordered (U(1) or SU(2) symmetry breaking) phases, such as the superfluid phase or Néel phase, it was found that $\ln |X_M(\theta)| \sim -bL \ln L$ [11, 57]. At the quantum critical points of 2D lattice models, previous studies [11, 55, 57] showed that $\ln |X_M(\theta)|$ takes the following general form for a rectan-

gle region M :

$$\ln |X_M(\theta)| = -a_1 L + s \ln(L) + a_0, \quad (7)$$

where all the coefficients are functions of θ and the log-coefficient s follows a universal function of both θ and the opening angles of the corners of M ($\pi/2$ for rectangle region). Given a smooth region (without a corner), there should be no corner correction and the log-coefficient $s = 0$. Such area-law decay of disorder operator, i.e. $\ln |X_M(\theta)| = -a_1 L + a_0$, holds both at the QCP and inside the gapped symmetric phases.

To detect the scaling of the disorder operator at the quantum phase transition point of EPJQ model in Eq. (1), we choose the entanglement region M to be a $L \times L/2$ cylinder region (without corner) in the lattice, as shown in the right inset of Fig. 1 (a), with system size for $L = 8$ up to $L = 144$. For a good comparison, we calculated the U(1) disorder operator (with small rotation angle $\theta = 0.2$) for the Néel phase (standard spin-1/2 Heisenberg model on the square lattice), the O(3) QCP of $J_1 - J_2$ model in Eq. (6), DQCP of JQ₃ model (Eq. (1) at $\Delta = 1$), and quantum phase transition points of EPJQ of Eq. (1) for $\Delta = 0, 0.1, 0.3, 0.5$, respectively. The results are shown in Fig. 3 (a).

As the leading term of the U(1) disorder operator X_M at small θ for the Néel phase is $\ln |X_M(\theta)| \sim -bL \ln L$, one expects $\ln |X_M(\theta)|/L$ proportional to $\ln L$ with a pronounced slope, as shown in Fig. 3 (a). For the (2+1)D O(3) QCP of $J_1 - J_2$ model, since $\ln |X_M(\theta)| \sim L$ with log-coefficient $s = 0$ due to the smooth boundary, and $\ln |X_M(\theta)|/L$ will be a constant at large system size, which is also clearly seen in Fig. 3 (a).

The case for the DQCP of JQ₃, $\ln |X_M(\theta)|/L$ as a function of $\ln L$ gives a tiny slope, signifying the anomalous scaling coming from the very weak Goldstone mode contribution

at the weakly first-order transition [11]. But interestingly, one clearly sees that the slopes of $\ln|X_M(\theta)|/L$ became sharper at the first-order phase transition points of EPJQ, especially as anisotropy $\Delta \rightarrow 0$ as shown in the inset of Fig. 3 (a) for $\Delta = 0.5, 0.3, 0.1$ and 0. Therefore, the scaling behavior of disorder operator reveals the residual Néel orders and first-order nature of the transition of EPJQ model, connecting the situation from $\Delta = 1$ to $\Delta = 0$.

We have further computed a related quantity – the bipartite spin fluctuation [63]. At $\theta \rightarrow 0$ limit, the scaling of the disorder operator $-\ln|X_M|$ has a similar behavior to that of the bipartite spin fluctuations, which is defined as

$$F_M = \langle (S_M^z - \langle S_M^z \rangle)^2 \rangle, \quad S_M^z = \sum_{i \in M} S_i^z. \quad (8)$$

So at the Néel phase, the scaling of the bipartite fluctuations is $F_M \sim bL \ln L$ [32, 63], and $F_M/L \sim b \ln L$ as show in Fig. 3 (b). For the (2+1)D O(3) QCP of $J_1 - J_2$ model, the bipartite spin fluctuations of the smooth region have a linear scaling $F_M \sim aL$ and F_M/L will be a constant at large system size L . Turn to the DQCP of JQ₃ model, F_M/L as a function of $\ln L$ gives a tiny slope at large system size L , consistent with that of the disorder operator in Fig. 3 (a) and our previous observation of anomalous log-coefficient [11]. More interestingly, the slopes of F_M/L versus $\ln L$ also became sharper at the phase transition points of the EPJQ with $\Delta = 0.5, 0.3, 0.1$ and 0, especially at large system sizes and anisotropy $\Delta \rightarrow 0$ as highlighted by dashed rectangular boxes of Fig. 3 (b). The scaling at large size reveals similar behavior as that of Néel orders contributed from the remaining Goldenstone mode. This evolution further strengthens the understanding that the DQCP transitions change from weak to prominent first-order transitions from $\Delta = 1$ to $\Delta = 0$.

IV. ENTANGLEMENT ENTROPY

Next we investigate the EE at the transition points of various Δ of Eq. (1). To this end, we employ the nonequilibrium increment method [12, 64–66] within the framework of SSE-QMC simulation [42, 43] to determine the second Rényi entropy of the EPJQ model at phase transition points for various values of Δ . Rényi entanglement entropy is defined as $S_A^{(n)} = \frac{1}{1-n} \ln \text{Tr} \rho_A^n$ which can be reexpressed in the form of $S_A^{(n)} = \frac{1}{1-n} \ln \frac{Z_A^{(n)}}{Z^{(n)}}$ according to the replica trick [67]. The nonequilibrium method is based on Jarzynski's equality [68], which relates the free energy difference between two systems with the total work done during a tuning process from one system to another. We regard the partition functions $Z_A^{(n)}$ and $Z^{(n)}$ as those of two different physical systems, then it is natural to apply the Jarzynski's equality and design a tuning process between the two systems to calculate

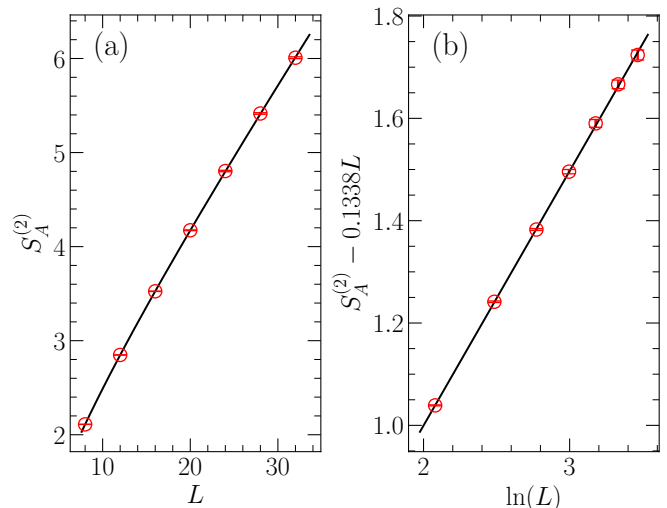


FIG. 4. Second Rényi entropy $S_A^{(2)}$ for $L \times L$ lattice with subsystem size of $L/2 \times L$ deep in the AFX phase of EPJQ model at $\Delta = 0$ and $q = 0.3$. (a) $S_A^{(2)}$ versus system size L . The black curve is a fit to $S_A^{(2)} = aL + b \ln(L) + c$ and the fitting result is $S_A^{(2)} = 0.1338(8)L + 0.497(11) \ln(L) + 0.0046(166)$. (b) $S_A^{(2)} - aL$ vs. $\ln(L)$ for different system sizes where we choose the fitted value $a = 0.1338$. The black curve is a straight line of $y = 0.497x + 0.0046$.

the Rényi entropies [64, 65]. In practice, we follow the incremental version [12, 66] of Ref. [65], and it can overcome the fact that the EE is in general an exponential observable [69, 70]. We conduct the simulation on a $L \times L$ square lattice with periodic boundary conditions, and fix with $\beta = L$ and choose the subregion A to be a $L \times L/2$ cylinder defined same as region M in the right inset of Fig. 1 (a), which has no sharp corners on the entanglement boundary.

For $\Delta < 1.0$, in the AFX phase, the system spontaneously breaks the SO(2) spin symmetry and exhibits one Goldstone mode. In this case, the entanglement entropy (EE) is expected to scale as [32]

$$S_A^{(n)} = aL + b \ln(L) + c, \quad b = \frac{N_g}{2}, \quad (9)$$

where N_g represents the number of Goldstone modes. Eq. (9) has been verified for both XY and Néel ordered states, which have one and two Goldstone modes [13, 65, 66, 70–74], respectively. We first test our algorithm in the AFX phase of the EPJQ model at $\Delta = 0$ and $q = 0.3 \ll q_c$, with the results displayed in Fig. 4. We measure the second order Rényi EE for the subsystem M. The system sizes utilized are $L = 8, 12, 16, \dots, 32$ and the temperature is fixed at $\beta = L$. As shown in Fig. 4(b), by fitting to Eq. (9), we observe a good agreement between our data with the scaling form of Eq. (9). Moreover, the log-coefficient obtained from curve fitting is $\frac{N_g}{2} = 0.497 \pm 0.011$, aligning well with the expectation of existence of one Goldstone mode, which corresponds to

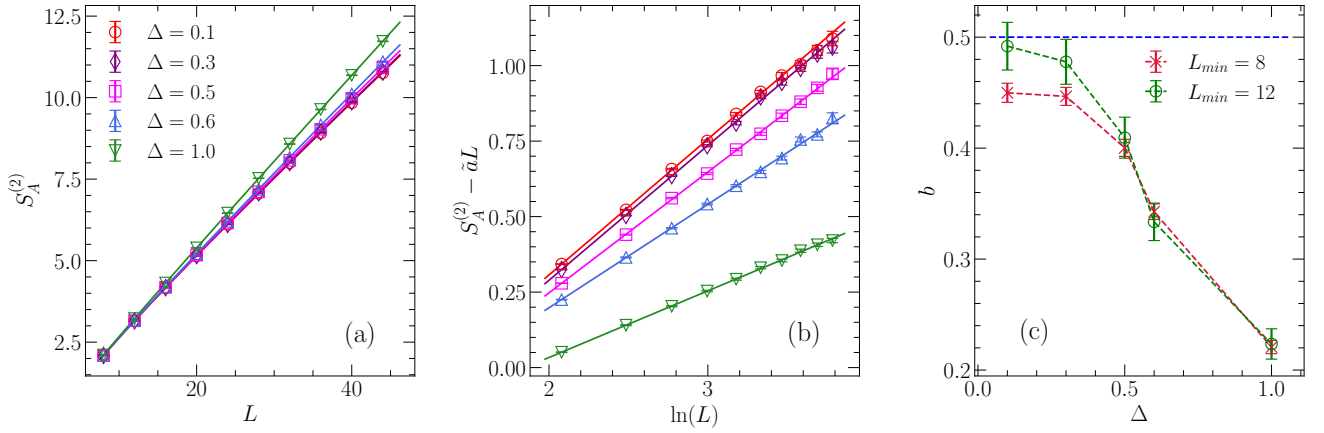


FIG. 5. Second Rényi entropy $S_A^{(2)}$ for $L \times L$ lattice with subsystem size of $L/2 \times L$ at the phase transitions of EPJQ model for different anisotropy Δ as in Table. I and $\Delta = 1$ of JQ model. (a) $S_A^{(2)}$ versus L for different Δ . The solid lines are fitted curves of finite-size data according to Eq. (9). (b) $S_A^{(2)} - \tilde{a}L$ versus $\ln(L)$ for different Δ . $\tilde{a} = a(\Delta)$ is the fitted area law coefficient a for different Δ . (c) The fitted log-coefficient b versus Δ . We gradually exclude the data for small system sizes, and L_{\min} is the smallest system size used in the fitting process. The blue dotted line is a guide for eyes, indicating $b = 0.5$ or $N_G = 1$.

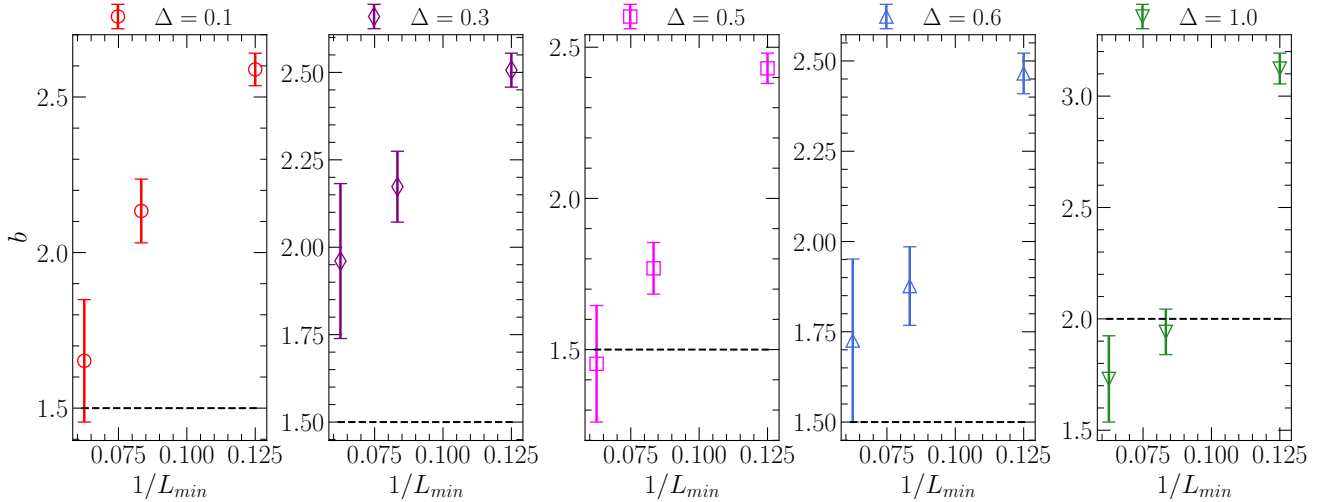


FIG. 6. Fitted log-coefficient b according to Eq. (10) with finite-size data of $\rho_s(L)$ and $I(L)$ obtained from QMC simulations at the phase transition points of EPJQ model for different Δ . By considering the finite size values of $\rho_s(L)$ and $I(L)$, the obtained b indeed gets enhanced, although with larger error bars. The black dotted lines are guides for eyes for the log coefficient of three Goldstone modes from the $SO(4)$ symmetry-breaking (for $\Delta < 1$) and four Goldstone modes from the $SO(5)$ symmetry-breaking (for $\Delta = 1$) cases.

spontaneous $SO(2)$ symmetry breaking. The analysis of the fitting quality can be found in the Sec. II in SM [46].

We then proceed to the phase transition points. Our extrapolated finite order parameter data in Fig. 1(b) shows that the first-order behavior is more pronounced as Δ decreases from 1 to 0. However, the relation between the scaling of entanglement entropy (EE) with the strengthen of first-order behavior remains unexplored. We measure the second Rényi EE at the transition points in Table. I for various values of Δ and system sizes $L = 8, 12, 16, \dots, 44$ and fix $\beta = L$. The results are presented in Fig. 5. For all examined values of Δ , we observe a clear logarithmic correction to the area law term

in the scaling of EE (Eq. (9)). Additionally, as Δ decreases and the first-order behavior strengthens, the fitted log-coefficient b increases. Interestingly, for $\Delta = 0.1$ and $\Delta = 0.3$, the fitted value of b is even consistent with 0.5, which corresponds to the existence of a single Goldstone mode, the same as the scaling of EE deep inside the AFXY phase in Fig. 4. Our findings suggest that at least for $\Delta \leq 0.3$ the log-coefficient b characterizes an evident first order transition with $SO(2)$ symmetry breaking associated with one Goldstone mode.

At $\Delta = 1.0$, where the system reduces to the isotropic JQ_3 model, it has been discovered that even with a smooth entanglement boundary, the system exhibits

anomalous positive logarithmic subleading corrections, resembling the Goldstone mode contribution, while the coefficient is only around 0.2-0.3 [13, 14]. In addition, a recent study [33] considers carefully the finite-size effects in Eq. (9), and use the modified fitting function for Goldstone mode phase

$$S_A^{(2)}(L) = aL + \frac{n_G}{2} \ln \left[(\rho_s(L)L)^{1/2} (I(L)L)^{1/2} \right] + c, \quad (10)$$

where $\rho_s(L)$ is the finite-size spin stiffness and $I(L)$ the finite-size transverse spin susceptibility. Through this procedure, the log-coefficient is fitted to be around 2 which corresponds to four Goldstone modes [33]. This is used to suggest that the system breaks the emergent SO(5) symmetry at the transition point, and this process can be well detected by the scaling of EE even at relatively small system sizes.

We followed this procedure, calculated the finite-size spin stiffness $\rho_s(L)$ and transverse spin susceptibility $I(L)$, and substituted them in Eq. (10), same as in Ref. [33] to fit our EE data. However, as shown in Fig. 6, we find it is not so easy to observe the same convergence of log-coefficient to 2 at $\Delta = 1.0$ or to 1.5 at $\Delta < 1.0$, which would suggest the breaking of emergent SO(5) (four Goldstone modes) and SO(4) (three Goldstone modes) symmetries, respectively. In fact, at $\Delta = 1.0$ the last two data points with larger L_{\min} are quite close to $b = 2$, although the last data point slightly deviates below $b = 2$.

For $\Delta < 1.0$, except for $\Delta = 0.3$, the last data points all seem to be consistent with $b = 1.5$. However, within our limited data quality, we do not observe the stability of fitted results with respect to L_{\min} for any Δ . It is possible that our results can be affected by stronger finite-size effects as we fixed $\beta = L$ to approach the thermodynamic limit, while Ref. [33] used the projector quantum Monte Carlo [75, 76] to simulate the ground state of the system and fix the projection power to be $m = L^3$. But we think physically the more important point is, that we observed at $\Delta < 1.0$ the first order is enhanced, so that the emergent SO(4) behavior can be weakened at the system sizes we considered, and a strong first-order behavior with only one Goldstone mode might be mixed with the SO(4) symmetry breaking behavior with three Goldstone modes. In this case, the fitted log coefficient with Eq. (10) for $\Delta < 1.0$ could drift significantly from 1.5 to 0.5 when larger system sizes are considered. We therefore think that overall our fitting results with Eq. (10) are consistent with Ref. [33] for JQ₃ model and show the capability of EE in characterizing the emergent symmetry and weakly first order behaviors at the complicated DQCPs.

V. DISCUSSION

Our work shows the two non-local measurements – the disorder operator and entanglement entropy – consis-

tently exhibit anomalous scaling behaviors at the easy-plane deconfined quantum criticalities. By adjusting the anisotropy from the Heisenberg limit ($\Delta = 1$) to the easy-plane limit ($\Delta = 0$), we find that as the first-order nature of the transition is being amplified, the anomalous behavior of both the disorder operator and entanglement entropy becomes more apparent, resembling contributions from Goldstone modes. Interestingly, when $\Delta \leq 0.3$, the log coefficient in EE seem to converge to $b = 0.5$ which is consistent with one Goldstone mode and SO(2) symmetry breaking at the first-order transition points. Additionally, when applying the finite-size fitting form of Goldstone mode phase (Eq. (10)) to fit our EE data, we obtain the enhanced log coefficients close to that of emergent SO(5) symmetry breaking at $\Delta = 1$ and emergent SO(4) symmetry breaking at $\Delta < 1$. However, the log coefficients do not show the good convergence behavior, as shown in Ref. [33], which maybe explained by insufficient data quality or very weak emergent SO(4) symmetry at $\Delta < 1$ due to the strengthening of first order behavior. Our work thus provides strong evidence that the observed anomalous scaling behaviors of the entanglement measurements (disorder operator and EE) indeed come from the weakly-first-order nature of DQCPs of JQ model realizations both at $\Delta = 1$ and $\Delta < 1$.

Note that our work and previous studies [11–17, 33, 38] on the EE scaling of smooth cut on a square lattice are not contradicted with the recent work by D’Emidio and Sandvik [38] where they consider a $\frac{\pi}{4}$ -degrees-tilted square lattice and observe the normal scaling of EE obeying the requirements of CFTs. We think the cut dependence of EE actually supports the transition is indeed weakly-first order and the tilted cut and standard cut possibly just capture the two sides of the JQ-type DQCP story. On the one hand, it is a weakly first transition which can be detected by the standard cut, and on the other hand the system might be close to a real continuous transition so that the tilted cut captures some essential information of the CFT at small system sizes. In conclusion, scaling of these nonlocal observables have proven to be both powerful and sensitive tools in characterising this kind of weakly first-order transitions [11–13, 33], and it provides strong evidence that the JQ type DQCP is weakly first order however very close to a real continuous transition [44], possibly of multicritical type related with the SO(5) model with Wess-Zumino-Witten term [44, 48, 77–79] or the ‘walking’ pseudo-criticality behavior at the transition [34–37].

Future research directions may include investigating the disorder operator and entanglement entropy scaling of JQ_n models with $n > 3$, which have been shown to exhibit stronger first-order transitions [44, 80] as n increases, similar to EPJQ models. Another avenue of interest is to explore the entanglement entropy scaling of an absolutely strong first-order transition, which involves a mixture of two phases with classical probabilities. Moreover, multipartite entanglement [81–84] and higher-order Rényi entropies, entanglement negativity and entangle-

ment spectrum [85–87] with QMC simulations at the DQCP also present intriguing topics for future investigation.

ACKNOWLEDGEMENT

We thank Meng Cheng, Cenke Xu, Anders Sandvik, Senthil Todadri, Subir Sachdev for valuable discussions on the related topic. NVM and ZYM acknowledge the earlier insightful discussions on the transitions of EPJQ model with Arnab Sen and Anders Sandvik. JRZ and ZYM acknowledge the support from the Research Grants Council (RGC) of Hong Kong Special Administrative Region of China (Project Nos. 17301721, AoE/P-701/20, 17309822, HKU C7037- 22GF, 17302223), the ANR/RGC Joint Research Scheme sponsored by RGC of Hong Kong and French National Re-

search Agency (Project No. A HKU703/22), the GD-NSF (No. 2022A1515011007) and the HKU Seed Funding for Strategic Interdisciplinary Research. Y.C.W. acknowledges the support from Zhejiang Provincial Natural Science Foundation of China (Grant No. LZ23A040003), and the support from the High-Performance Computing Centre of Hangzhou International Innovation Institute of Beihang University. NVM acknowledge the National Natural Science Foundation of China (No. 12004020) and the Fundamental Research Funds for the Central Universities. We thank HPC2021 system under the Information Technology Services and the Blackbody HPC system at the Department of Physics, University of Hong Kong, as well as the Beijing PARATERA Tech CO.,Ltd. (URL: <https://cloud.paratera.com>) for providing HPC resources that have contributed to the research results reported within this paper.

-
- [1] T. Senthil, *Science* **303**, 1490–1494 (2004).
- [2] T. Senthil, L. Balents, S. Sachdev, A. Vishwanath, and M. P. A. Fisher, *Phys. Rev. B* **70**, 144407 (2004).
- [3] M. Levin and T. Senthil, *Physical Review B* **70**, 220403 (2004).
- [4] T. Senthil, L. Balents, S. Sachdev, A. Vishwanath, and M. P. A. Fisher, *Journal of the Physical Society of Japan* **74**, 1 (2005), <https://doi.org/10.1143/JPSJS.74S.1>.
- [5] K. Harada, T. Suzuki, T. Okubo, H. Matsuo, J. Lou, H. Watanabe, S. Todo, and N. Kawashima, *Physical Review B* **88**, 220408 (2013).
- [6] K. Chen, Y. Huang, Y. Deng, A. B. Kuklov, N. V. Prokof'ev, and B. V. Svistunov, *Phys. Rev. Lett.* **110**, 185701 (2013).
- [7] A. Nahum, J. Chalker, P. Serna, M. Ortuño, and A. Somoza, *Physical Review X* **5**, 041048 (2015).
- [8] Y. Nakayama and T. Ohtsuki, *Phys. Rev. Lett.* **117**, 131601 (2016).
- [9] Z. Li, *JHEP* **11**, 005 (2022), [arXiv:1812.09281 \[hep-th\]](https://arxiv.org/abs/1812.09281).
- [10] D. Poland, S. Rychkov, and A. Vichi, *Rev. Mod. Phys.* **91**, 015002 (2019).
- [11] Y.-C. Wang, N. Ma, M. Cheng, and Z. Y. Meng, *SciPost Phys.* **13**, 123 (2022).
- [12] J. Zhao, Y.-C. Wang, Z. Yan, M. Cheng, and Z. Y. Meng, *Phys. Rev. Lett.* **128**, 010601 (2022).
- [13] M. Song, J. Zhao, Z. Y. Meng, C. Xu, and M. Cheng, [arXiv e-prints](https://arxiv.org/abs/2312.13498), [arXiv:2312.13498 \(2023\)](https://arxiv.org/abs/2312.13498), [arXiv:2312.13498 \[cond-mat.str-el\]](https://arxiv.org/abs/2312.13498).
- [14] M. Song, J. Zhao, M. Cheng, C. Xu, M. M. Scherer, L. Janssen, and Z. Y. Meng, [arXiv e-prints](https://arxiv.org/abs/2307.02547), [arXiv:2307.02547 \(2023\)](https://arxiv.org/abs/2307.02547), [arXiv:2307.02547 \[cond-mat.str-el\]](https://arxiv.org/abs/2307.02547).
- [15] Z. H. Liu, W. Jiang, B.-B. Chen, J. Rong, M. Cheng, K. Sun, Z. Y. Meng, and F. F. Assaad, *Phys. Rev. Lett.* **130**, 266501 (2023).
- [16] Y. D. Liao, G. Pan, W. Jiang, Y. Qi, and Z. Y. Meng, [arXiv e-prints](https://arxiv.org/abs/2302.11742), [arXiv:2302.11742 \(2023\)](https://arxiv.org/abs/2302.11742), [arXiv:2302.11742 \[cond-mat.str-el\]](https://arxiv.org/abs/2302.11742).
- [17] Z. H. Liu, Y. Da Liao, G. Pan, M. Song, J. Zhao, W. Jiang, C.-M. Jian, Y.-Z. You, F. F. Assaad, Z. Y. Meng, and C. Xu, *Phys. Rev. Lett.* **132**, 156503 (2024).
- [18] M. Zayed, C. Rüegg, J. Larrea J, A. Läuchli, C. Panagopoulos, S. Saxena, M. Ellerby, D. McMorro, T. Strässle, S. Klotz, G. Hamel, R. A. Sadykov, V. Pomjakushin, M. Boehm, M. Jiménez–Ruiz, A. Schneidewind, E. Pomjakushina, M. Stingaciu, C. K., and H. M. Rønnow, *Nature physics* **13**, 962 (2017).
- [19] J. Guo, G. Sun, B. Zhao, L. Wang, W. Hong, V. A. Sidorov, N. Ma, Q. Wu, S. Li, Z. Y. Meng, A. W. Sandvik, and L. Sun, *Phys. Rev. Lett.* **124**, 206602 (2020).
- [20] J. L. Jiménez, S. P. G. Crone, E. Fogh, M. E. Zayed, R. Lortz, E. Pomjakushina, K. Conder, A. M. Läuchli, L. Weber, S. Wessel, A. Honecker, B. Normand, C. Rüegg, P. Corboz, H. M. Rønnow, and F. Mila, *Nature* **592**, 370 (2021).
- [21] G. Sun, N. Ma, B. Zhao, A. W. Sandvik, and Z. Y. Meng, *Chinese Physics B* **30**, 067505 (2021).
- [22] Y. Cui, L. Liu, H. Lin, K.-H. Wu, W. Hong, X. Liu, C. Li, Z. Hu, N. Xi, S. Li, R. Yu, A. W. Sandvik, and W. Yu, *Science* **380**, 1179 (2023).
- [23] J. Guo, P. Wang, C. Huang, B.-B. Chen, W. Hong, S. Cai, J. Zhao, J. Han, X. Chen, Y. Zhou, S. Li, Q. Wu, Z. Y. Meng, and L. Sun, [arXiv e-prints](https://arxiv.org/abs/2310.20128), [arXiv:2310.20128 \(2023\)](https://arxiv.org/abs/2310.20128), [arXiv:2310.20128 \[cond-mat.str-el\]](https://arxiv.org/abs/2310.20128).
- [24] A. W. Sandvik, *Phys. Rev. Lett.* **98**, 227202 (2007).
- [25] J. Lou, A. W. Sandvik, and N. Kawashima, *Phys. Rev. B* **80**, 180414 (2009).
- [26] H. Shao, W. Guo, and A. W. Sandvik, *Science* **352**, 213 (2016).
- [27] N. Ma, G.-Y. Sun, Y.-Z. You, C. Xu, A. Vishwanath, A. W. Sandvik, and Z. Y. Meng, *Phys. Rev. B* **98**, 174421 (2018).
- [28] Y. Q. Qin, Y.-Y. He, Y.-Z. You, Z.-Y. Lu, A. Sen, A. W. Sandvik, C. Xu, and Z. Y. Meng, *Phys. Rev. X* **7**, 031052 (2017).
- [29] H. Casini and M. Huerta, *Journal of High Energy Physics* **2012**, 87 (2012).
- [30] E. Fradkin and J. E. Moore, *Phys. Rev. Lett.* **97**, 050404 (2006).

- [31] H. Casini and M. Huerta, *Nucl. Phys. B* **764**, 183–201 (2007).
- [32] M. A. Metlitski and T. Grover, (2015), [arXiv:1112.5166 \[cond-mat.str-el\]](#).
- [33] Z. Deng, L. Liu, W. Guo, and H.-q. Lin, [arXiv e-prints](#), [arXiv:2401.12838](#) (2024), [arXiv:2401.12838 \[cond-mat.str-el\]](#).
- [34] C. Wang, A. Nahum, M. A. Metlitski, C. Xu, and T. Senthil, *Physical Review X* **7**, 031051 (2017).
- [35] A. Nahum, *Phys. Rev. B* **102**, 201116 (2020).
- [36] R. Ma and C. Wang, *Phys. Rev. B* **102**, 020407 (2020).
- [37] Z. Zhou, L. Hu, W. Zhu, and Y.-C. He, [arXiv preprint arXiv:2306.16435](#) (2023).
- [38] J. D’Emidio and A. W. Sandvik, [arXiv e-prints](#), [arXiv:2401.14396](#) (2024), [arXiv:2401.14396 \[cond-mat.str-el\]](#).
- [39] N. Ma, Y.-Z. You, and Z. Y. Meng, *Phys. Rev. Lett.* **122**, 175701 (2019).
- [40] B. Zhao, P. Weinberg, and A. W. Sandvik, *Nature Physics* **15**, 678 (2019).
- [41] N. Desai and R. K. Kaul, *Phys. Rev. B* **102**, 195135 (2020).
- [42] A. W. Sandvik, *Phys. Rev. B* **59**, R14157 (1999).
- [43] O. F. Syljuåsen and A. W. Sandvik, *Phys. Rev. E* **66**, 046701 (2002).
- [44] J. Takahashi, H. Shao, B. Zhao, W. Guo, and A. W. Sandvik, [arXiv e-prints](#), [arXiv:2405.06607](#) (2024), [arXiv:2405.06607 \[cond-mat.str-el\]](#).
- [45] Z. Deng, L. Liu, W. Guo, and H. Q. Lin, *Phys. Rev. B* **108**, 125144 (2023).
- [46] Determination of the transition points and extrapolations of the order parameters, and the analysis of the quality of the fitting in EE data are presented in this Supplemental Material.
- [47] N. Ma, P. Weinberg, H. Shao, W. Guo, D.-X. Yao, and A. W. Sandvik, *Phys. Rev. Lett.* **121**, 117202 (2018).
- [48] B.-B. Chen, X. Zhang, Y. Wang, K. Sun, and Z. Y. Meng, [arXiv e-prints](#), [arXiv:2307.05307](#) (2023), [arXiv:2307.05307 \[cond-mat.str-el\]](#).
- [49] K. Binder and D. P. Landau, *Phys. Rev. B* **30**, 1477 (1984).
- [50] F. Wegner, *J. Math. Phys.* **12**, 2259 (1971).
- [51] L. P. Kadanoff and H. Ceva, *Phys. Rev. B* **3**, 3918 (1971).
- [52] E. Fradkin, *Journal of Statistical Physics* **167**, 427 (2017).
- [53] Z. Nussinov and G. Ortiz, *Proceedings of the National Academy of Sciences* **106**, 16944 (2009).
- [54] Z. Nussinov and G. Ortiz, *Annals of Physics* **324**, 977 (2009).
- [55] J. Zhao, Z. Yan, M. Cheng, and Z. Y. Meng, *Phys. Rev. Res.* **3**, 033024 (2021).
- [56] X.-C. Wu, W. Ji, and C. Xu, *Journal of Statistical Mechanics: Theory and Experiment* **2021**, 073101 (2021).
- [57] Y.-C. Wang, M. Cheng, and Z. Y. Meng, *Phys. Rev. B* **104**, L081109 (2021).
- [58] X.-C. Wu, C.-M. Jian, and C. Xu, *SciPost Phys.* **11**, 033 (2021).
- [59] B.-B. Chen, H.-H. Tu, Z. Y. Meng, and M. Cheng, *Phys. Rev. B* **106**, 094415 (2022).
- [60] W. Jiang, B.-B. Chen, Z. H. Liu, J. Rong, F. F. Assaad, M. Cheng, K. Sun, and Z. Y. Meng, *SciPost Phys.* **15**, 082 (2023).
- [61] K.-L. Cai and M. Cheng, [arXiv e-prints](#), [arXiv:2404.04334](#) (2024), [arXiv:2404.04334 \[cond-mat.str-el\]](#).
- [62] X.-C. Wu, [arXiv e-prints](#), [arXiv:2404.04331](#) (2024), [arXiv:2404.04331 \[cond-mat.str-el\]](#).
- [63] H. F. Song, N. Laflorencie, S. Rachel, and K. Le Hur, *Phys. Rev. B* **83**, 224410 (2011).
- [64] V. Alba, *Phys. Rev. E* **95**, 062132 (2017).
- [65] J. D’Emidio, *Phys. Rev. Lett.* **124**, 110602 (2020).
- [66] J. Zhao, B.-B. Chen, Y.-C. Wang, Z. Yan, M. Cheng, and Z. Y. Meng, *npj Quantum Materials* **7**, 69 (2022).
- [67] P. Calabrese and J. Cardy, *Journal of Statistical Mechanics: Theory and Experiment* **2004**, P06002 (2004).
- [68] C. Jarzynski, *Phys. Rev. Lett.* **78**, 2690 (1997).
- [69] X. Zhang, G. Pan, B.-B. Chen, K. Sun, and Z. Y. Meng, *Phys. Rev. B* **109**, 205147 (2024).
- [70] X. Zhou, Z. Y. Meng, Y. Qi, and Y. Da Liao, *Phys. Rev. B* **109**, 165106 (2024).
- [71] J. Helmes and S. Wessel, *Phys. Rev. B* **89**, 245120 (2014).
- [72] B. Kulchytskyy, C. M. Herdman, S. Inglis, and R. G. Melko, *Phys. Rev. B* **92**, 115146 (2015).
- [73] Z. Deng, L. Liu, W. Guo, and H. Q. Lin, *Phys. Rev. B* **108**, 125144 (2023).
- [74] J. D’Emidio, R. Orús, N. Laflorencie, and F. de Juan, *Phys. Rev. Lett.* **132**, 076502 (2024).
- [75] A. W. Sandvik, *AIP Conference Proceedings* **1297**, 135 (2010), <https://aip.scitation.org/doi/pdf/10.1063/1.3518900>.
- [76] A. W. Sandvik, *Phys. Rev. Lett.* **95**, 207203 (2005).
- [77] B. Zhao, J. Takahashi, and A. W. Sandvik, *Phys. Rev. Lett.* **125**, 257204 (2020).
- [78] S. M. Chester and N. Su, *Phys. Rev. Lett.* **132**, 111601 (2024).
- [79] B.-B. Chen, X. Zhang, and Z. Y. Meng, [arXiv e-prints](#), [arXiv:2405.04470](#) (2024), [arXiv:2405.04470 \[cond-mat.str-el\]](#).
- [80] J. Takahashi and A. W. Sandvik, *Phys. Rev. Res.* **2**, 033459 (2020).
- [81] T. J. Osborne and M. A. Nielsen, *Phys. Rev. A* **66**, 032110 (2002).
- [82] Y. Javanmard, D. Trapin, S. Bera, J. H. Bardarson, and M. Heyl, *New Journal of Physics* **20**, 083032 (2018).
- [83] T.-T. Wang, M. Song, L. Lyu, W. Witczak-Krempa, and Z. Y. Meng, [arXiv e-prints](#), [arXiv:2402.14916](#) (2024), [arXiv:2402.14916 \[cond-mat.str-el\]](#).
- [84] G. Parez and W. Witczak-Krempa, [arXiv e-prints](#), [arXiv:2402.06677](#) (2024), [arXiv:2402.06677 \[quant-ph\]](#).
- [85] K.-H. Wu, T.-C. Lu, C.-M. Chung, Y.-J. Kao, and T. Grover, *Phys. Rev. Lett.* **125**, 140603 (2020).
- [86] F.-H. Wang and X. Y. Xu, [arXiv e-prints](#), [arXiv:2312.14155](#) (2023), [arXiv:2312.14155 \[cond-mat.str-el\]](#).
- [87] Z. Yan and Z. Y. Meng, *Nature Communications* **14**, 2360 (2023).

Supplemental Material for "Scaling of Disorder Operator and Entanglement Entropy at Easy-Plane Deconfined Quantum Criticalities"

I. THE CRITICALITY FOR DIFFERENT Δ IN THE EPJQ MODELS

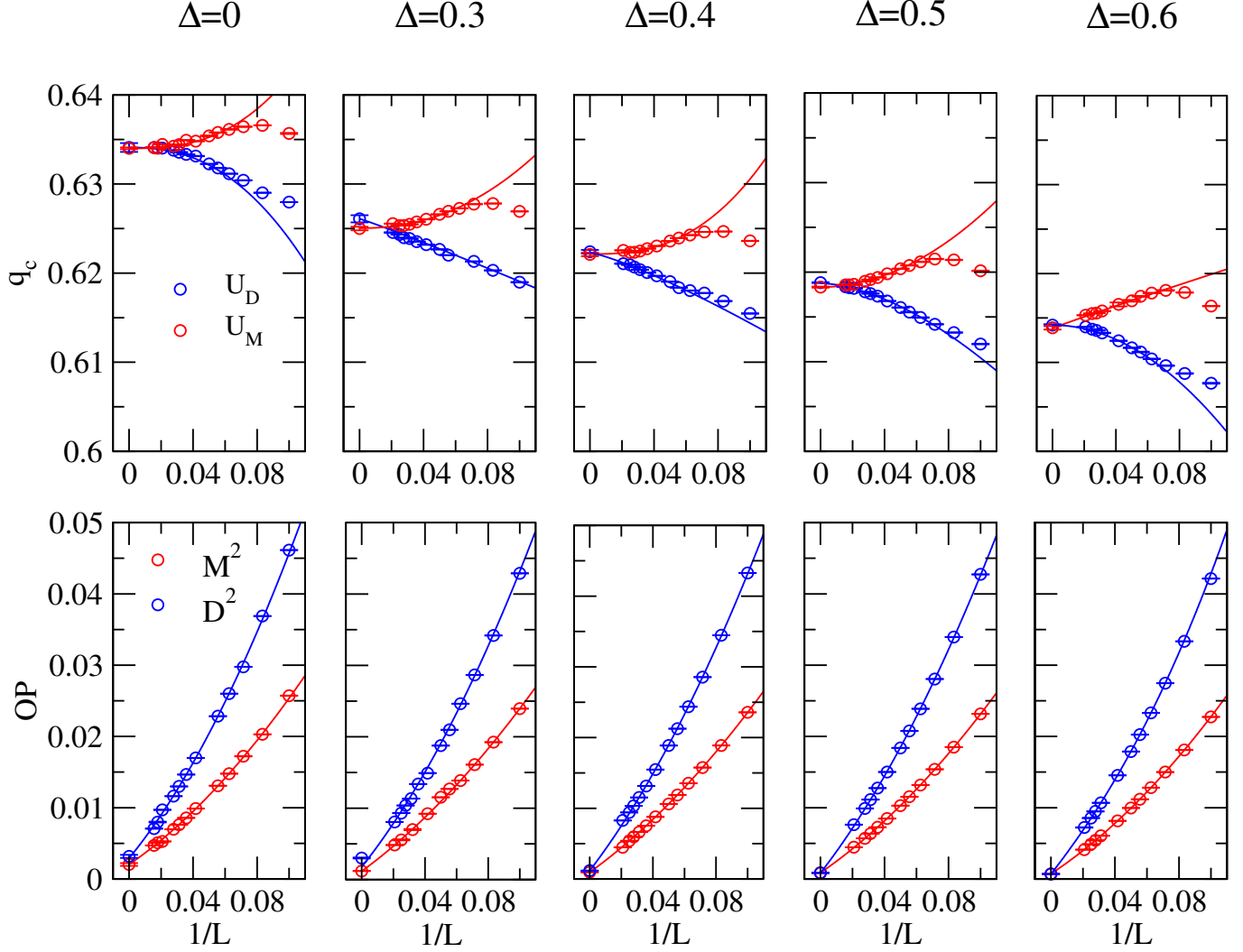


FIG. S1. (Upper panels) The crossing points $q_c(L)$ obtained from the curve of dimensionless Binder cumulants U_M (blue) and U_D (red) versus q close to the phase transition points for two system sizes L and $2L$. The red/blue curve is the fitting function with the scaling form of $q_c(L)$ in Eq. (5) excluding the crossings for small sizes with χ^2 of the fitting becomes close to one. The data points presented at $1/L = 0$ are the y-intercepts of fitting curves with the fitting errors which are given in Tab.I. (Lower panels) The value of order parameters for both AFX and VBS phases at $q_c(L)$ obtained with corresponding Binder cumulants versus $1/L$ in the EPJQ models with different Δ for all computing sizes L . The red/blue curve is the second-order polynomial fitting function of all the data points with χ^2 of the fitting close to one. The data points presented at $1/L = 0$ are the y-intercepts of the fitting curves with errors illustrated in Fig. 1.

The results in (b) of Fig. 1 in the main text present that the order parameters for both the AFX and VBS phases converge to a non-zero value when L goes to infinity for different Δ in the EPJQ models, which implies the possibility of first-order phase transitions in the EPJQ model. In this section we present the detail procedure in obtaining those converged order parameters at thermodynamic limit in Fig. 1(b). The binder cumulants U_M and U_D defined in Eq. (4)

for the AFXY and VBS phases correspondingly are two dimensionless quantities that are commonly chosen in the FSS of calculating critical points and correlation length exponents. In this paper we study the critical behavior of the EPJQ model with different anisotropic value Δ with the help of U_M and U_D all the crossing points $q_c(L)$ of two simulated sizes L and $2L$ got from U_M and U_D are shown in the first row in Fig. S1 for those different Δ . Using the fitting form in Eq. (5) two $q_c(\infty)$ can be got, which are listed in Tab.I in the main text. At each crossing point $q_c(L)$ we also calculate the square of order parameters defined in Eq. 2 and Eq. 3 as $M_x^2(L)$ and $D^2(L)$ illustrated in the second row in Fig. S1. It should be noticed that $M_x^2(L)$ and $D^2(L)$ are calculated at different $q_c(L)$ as the crossing points are got from different dimensionless quantities. In the calculation of $M_x^2(L)$ we chose the corresponding $q_c(L)$ got from U_M for two sizes L and $2L$. As for the $D^2(L)$ the crossing points are located using U_D . After all the $M_x^2(L)$ and $D^2(L)$ are known for different sizes, the square of order parameters at critical points when $L \rightarrow \infty$ can be calculated with the second-order polynomial fitting. All the fitting parameters of $M_x^2(\infty)$ and $D^2(\infty)$ for different Δ are illustrated in Fig. 1 in the main text.

II. COMPARISON OF FITTING QUALITY

In the main text, the scaling form of EE we use for the fitting is

$$S_A^{(2)} = aL + b \ln(L) + c. \quad (\text{S1})$$

However, to confirm the validity of the fitting form we use, we consider the comparison of above fitting form with the following one

$$S_A^{(2)} = aL + b/L + c, \quad (\text{S2})$$

which has no subleading L - dependence term but with a finite-size correction term b/L .

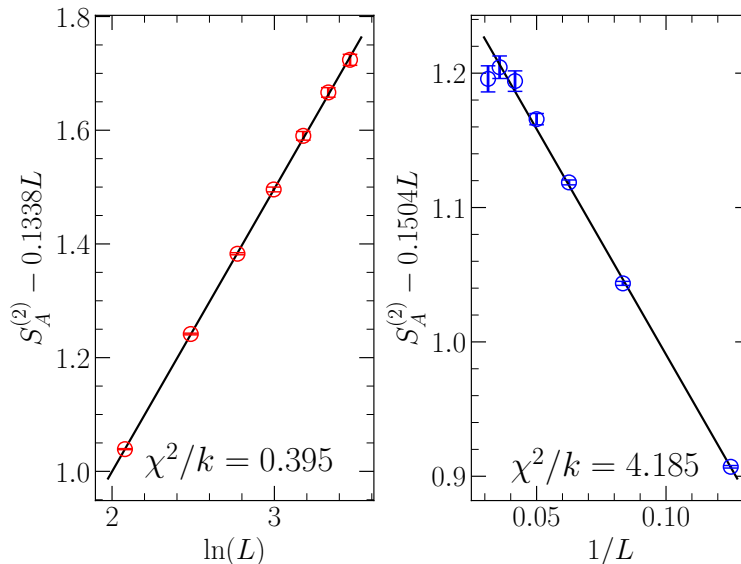


FIG. S2. Comparison of fitting quality with Eq. S1 and Eq. S2 in the AFMXY phase at $\Delta = 0$ and $q = 0.3$. Left panel: $S_A^{(2)} - 0.1338L$ versus $\ln(L)$ with area law coefficient obtained from fitting to Eq. S1. Right panel: $S_A^{(2)} - 0.1504L$ versus $1/L$ with area law coefficient obtained from fitting to Eq. S2. The chi-squared values of two fittings are also printed on the figure.

We use the chi-squared value χ^2/k to evaluate the fitting quality. chi-squared value is defined as

$$\chi^2 = \sum_{i=1}^N \frac{(f(x_i) - y_i)^2}{\sigma_i^2}, \quad (\text{S3})$$

where σ_i is the uncertainty of data y_i . $k = N - r$ is the effective number of degrees of freedom, where N is the number of data points and r is the number of fitting parameters. χ^2/k is expected to be close to 1 for a good fit. As shown in Fig. S2, in the AFMXY phase, the fitting quality is compared with Eq. S1 and Eq. S2 and the χ^2/k values are

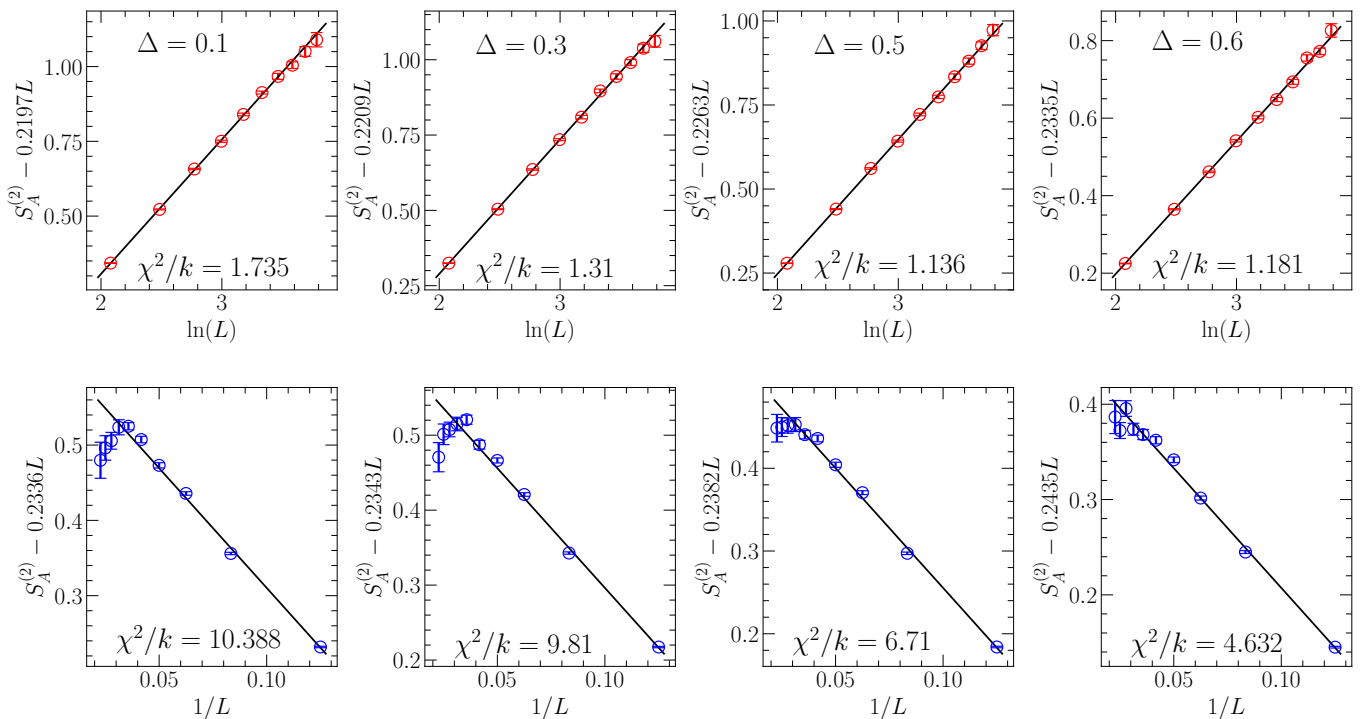


FIG. S3. Comparison of fitting quality with Eq. S1 and Eq. S2 at the DQCPs of easy-plane JQ_3 model. The red and blue data points represent the finite-size EE data with an area law term subtracted. The area law term is fitted from Eq. S1 for red data points and Eq. S2 for blue data points.

0.395 and 4.185 separately. χ^2/k should be typically distributed within the range $[1 - \sqrt{2/k}, 1 + \sqrt{2/k}]$ where for this case the range is $[0.465, 1.535]$. In our simulation, the precise estimation of statistic errors can be affected by limited number of Monte Carlo bins so that we attribute the small deviation of 0.395 to 0.465 to problematic errorbars and 4.185 is apparently far away from the ideal range. We thus conclude that Eq. S1 fits the data better than Eq. S2.

Similarly, for DQCPs of easy-plane JQ_3 model, the comparison of fitting quality with Eq. S1 and Eq. S2 is also performed and the results are shown in Fig. S3. By comparing their χ^2/k values, we conclude that Eq. S1 in all cases fit better than Eq. S2. Note that for $\Delta = 1.0$ which is the standard JQ_3 model, it has already been shown in previous study [13] that Eq. S1 fits the better. In that case we only present the comparison for $\Delta < 1.0$ in this manuscript.